IIETA International Information and Engineering Technology Association
Advancing the World of Information and Engineering

Journal Européen des Systèmes Automatisés
Vol. 59, No. 4, April, 2026, pp. 1111-1123
Journal homepage: http://iieta.org/journals/jesa

Passivity and Practical Stability of Fast-Sampled Quantized Discrete-Time Nonlinear Systems with Finite-Register Effects

Othman M. Hussein Anssari[1], Raoof Hazim Kareem[2], Abdullah Makki Jebur[2]

[1] ITRDC, University of Kufa, Al Najaf City 54001, Iraq
[2] Department of Electronic and Communications Engineering, College of Engineering, University of Kufa, Al Najaf City 54001, Iraq

Corresponding Author Email: Othman.alansari@uokufa.edu.iq

https://doi.org/10.18280/jesa.590421

Received: 8 January 2026
Revised: 19 March 2026
Accepted: 5 April 2026
Available online: 30 April 2026

Keywords:
discrete-time nonlinear systems, quantization, finite-precision effects, passivity, practical stability, sampled-data control, fast sampling

ABSTRACT

Digital implementation of nonlinear control laws inevitably introduces quantization, saturation, and finite-word-length arithmetic that can degrade nominal stability. This paper develops an implementation-aware passivity framework for fast-sampled discrete-time nonlinear systems subject to quantized measurements, quantized actuation, and finite-register effects. All implementation nonlinearities are aggregated into a single structured input perturbation, which is propagated through the plant Lipschitz bound and a dissipation-type storage function. Three main results are established: (i) semi-passivity of the implemented closed loop is preserved provided the degraded dissipation function remains positive outside a compact set; (ii) practical stability with an explicit ultimate bound is guaranteed when disturbances are bounded; and (iii) for polynomial dissipation functions, global attraction to a prescribed residual ball is obtained. Design-oriented inequalities are derived that directly relate the admissible sampling period, quantization step sizes, and finite-register parameters to a guaranteed residual stability bound. Numerical validation on three examples a scalar nonlinear benchmark, a two-dimensional nonlinear system, and a digitally controlled DC-DC buck converter confirms that the proposed framework correctly predicts the monotone ordering of residual set sizes across all implementation scenarios, with analytical bounds conservative by less than 15 percent, and demonstrates that the derived design inequalities directly govern the achievable voltage regulation accuracy as a function of ADC word-length and sampling rate selection in embedded digital controller implementations.

1. INTRODUCTION

Digital controllers for nonlinear systems are implemented using sampled measurements, zero-order holds, fixed- or floating-point arithmetic, and digitally generated control signals. These layers introduce non-ideal nonlinearities, namely quantization, saturation, overflow, and rounding, that are not visible in ideal continuous-time designs but can substantially alter closed-loop stability and performance. Ignoring such effects may lead to overly optimistic conclusions about robustness, especially for fast-sampled and implementation-sensitive systems. As the complexity of embedded control grows in modern engineering applications, the need for an analysis framework that explicitly treats digital implementation artifacts has become increasingly important.

The issue of degradation of digital implementation is not just a practical engineering issue. It poses some serious theoretical issues concerning the correlation between the ideal design of control and the digitally actualized one. In the implementation of a controller developed in ideal continuous or infinite-precision conditions by a digital processor, the nominal stability guarantees are typically lost or not as strong as they are in the analysis, unless the implementation effects are considered. This motivates a systematic analysis of the interaction between quantization, finite-record computing, and rapid sampling, in order to adjust the inertia and stability properties of discrete-time nonlinear closed-loop systems. The following systems have a rich literature combined into four clearly topic groups, as shown below:

1.1 Quantized control and sampled-data systems

The stability analysis of quantized control systems has been extensively studied for both linear and nonlinear plants. Early results established stability conditions for finite-level quantized discrete-time linear systems using Lyapunov methods [1, 2]. Subsequent works extended these results to nonlinear networked control systems with packet losses and probabilistic sampling [3], and to T-S fuzzy systems with quantized measurements and inputs using LMI techniques [4, 5]. A common limitation of these results is that they either assume a known plant structure or restrict uncertainty to a specific class, which reduces their applicability to general nonlinear systems.

1.2 Interfered digital systems-quantization, overflow, and finite register effects

Another avenue of research models quantization and overflow nonlinearities as concatenated sector-bounded disturbances, and studies their joint influence on stability. Studies [6-9] presented a sequence of results for discrete-time systems with concatenated quantization and overflow nonlinearities, demonstrating that tighter stability bounds can be obtained by considering the effects together, rather than individually. Study [10] established fundamental results on finite word length effects in digital filters. These results are powerful, but are usually developed for filter-like systems, not closed-loop nonlinear control systems with explicit sampling structure.

1.3 Passivity-based analysis under digital implementation

Passivity theory is an attractive approach to address the robustness of control systems to implementation issues, because the supply rate structure can tolerate bounded inputs while retaining stability-like properties. Study [11] demonstrated preservation of quasi-passivity and ultimate boundedness under sampling and quantization of control when sampling period and quantization level meet certain criteria. Study [12] demonstrated practical coordination of passive agents under finite-level quantized measurement. For the Markovian jump systems, passivity-based filtering and stochastic sampled-data control were developed in studies [13-15] using the Lyapunov-Krasovskii functionals. Reference [16] studied passivity and stability for switched systems with quantization. Although these works make progress, none consider fast sampling and quantization effects (measurement, input, and finite-register effects) in a general nonlinear framework - the focus of this paper.

1.4 Fast-sampling and implementation-aware control

Fast-sampling discrete-time systems pose an extra challenge because the Lipschitz constants of the sampled plant dynamics increase with faster sampling, and this effects the state trajectory due to implementation errors. H∞ control for fast-sampling singularly perturbed systems was considered in [17, 18], and stabilization for fast-sampling singular Markovian systems was recently treated [19]. Impacts of sampled-data controller implementation, such as intersample behavior were investigated in the study [20]. Semi-passivity and practical stability for switched discrete-time nonlinear systems were shown to hold in the study [10], offering an alternative yet analogous result. The present paper builds on this work by explicitly identifying the relationship between fast-sampling, quantization resolution, and finite-register parameters through closed-form design inequalities. The proposed work is distinct in three ways. First, we consider both quantization and switching simultaneously with finite-register arithmetic. This paper treats all three implementation layers — measurement quantization, input quantization, and finite-word-length distortion — within a single perturbation structure. Second, the framework here applies to general nonlinear discrete-time systems without assuming a known plant structure or bounded uncertainty class. Third, the proposed framework is entirely deterministic and yields closed-form design inequalities that directly map implementation parameters to residual stability bounds, making it immediately usable for embedded digital controller design. The existing literature on quantized control, interfered digital systems, and passivity-based sampled-data systems does not provide a unified treatment that simultaneously covers fast sampling, measurement and input quantization, and finite-register effects within a single practical-stability framework for general nonlinear discrete-time systems. Available results either address specific plant classes such as T-S fuzzy or linear systems, or treat implementation errors as generic disturbances without deriving explicit design-oriented bounds relating sampling, quantization, and word-length to residual stability. This paper addresses this gap by developing an implementation-aware passivity analysis framework for fast-sampled discrete-time nonlinear systems. The central idea is to model all implementation nonlinearities as structured perturbations of the nominal closed-loop input, propagate them through the plant Lipschitz bound and storage function, and derive explicit inequalities that characterize how digital implementation modifies the system behavior.

The following are the key contributions of this paper:

A general fast-sampled discrete-time nonlinear closed-loop model is developed whereby the state and control signals are subject to static bounded-error quantizers and a finite-register interference operator, which reflects the most important nonlinearities of a digital implementation in a single perturbation structure. An explicit overall limit for execution error was obtained, which includes a combination of measurement quantization, input quantization, and limited log distortion in a small-disturbance estimation dependent on the state, with two constants directly related to the design parameters. The passivity-based analysis is constructed which reveals the way in which the implementation error alters the nominal storage inequality resulting in the new requirements on the semi-passivity preservation and practical stability of the implemented closed loop. Design inequalities are derived that depend on sampling period, quantization steps, and implementation parameters to a clear final bound on state trajectories, which gives practical guidelines of digital controller implementation. Numerical validation on three examples — a scalar nonlinear benchmark, a two-dimensional nonlinear system, and a digitally controlled DC-DC buck converter — confirms the theoretical predictions and demonstrates direct practical applicability of the design procedure of Section 4.6, showing explicitly how ADC resolution (8-bit, 12-bit, and 16-bit), sampling rate, and finite-register word-length determine the achievable voltage regulation accuracy in a realistic embedded power electronics control implementation. The remnant of the paper will follow this structure. Section 2 includes introductory symbols and terminology and the formulation of the problem. Section 3 establishes auxiliary parameters that constrain implementation errors and their impact on storage functions. Section 4 demonstrates and presents the main theories of quasi-passivity and operational stability, along with their design implications. Section 5 provides examples and a numerical simulation study, and Section 6 summarizes the paper and outlines future research directions.

2. PRELIMINARIES AND PROBLEM FORMULATION

2.1 Notation

Let $\mathbb{R}^n$ denotes by the n-dimensional Euclidean space, and

$\mathbb{Z} \geq 0$ the set of nonnegative integers, and for the vector $x \in \mathbb{R}^n$, $||x||$ denotes the Euclidean norm. in addition to a symmetric matrix $P = P^{\wedge}T \in \mathbb{R}\{n^{\times}n\}$, the notation $P > 0$ and $P \geq 0$ indicate positive definiteness and positive semi definiteness respectively, and $\lambda min(P)$ and $\lambda max(P)$ were denote its smallest, and largest eigenvalues.

$$\alpha_1, \alpha_2, \alpha_3 \; class \; K\infty \; definitions$$

2.2 Continuous-time plant and fast-sampled discrete-time model

Consider the nonlinear continuous-time plant:

$$dx/dt = f\_c\big(x(t), u(t), w(t)\big) \tag{1}$$

where, $x(t) \in R^n$ is the state, $u(t) \in R^m$ is the control input, and $w(t) \in R^n$ is an exogenous disturbance. The function fc: $\mathbb{R}^n \times \mathbb{R}^m \times \mathbb{R}^p \rightarrow \mathbb{R}^n$ represents the vector field of the continuous-time plant, which is assumed to be locally Lipschitz continuous in all arguments on the operating region of interest. No specific parametric form is imposed on f_c, so that the framework applies to any nonlinear system satisfying the stated Lipschitz and dissipation conditions. The discrete-time representation obtained under zero-order hold and sampling period $T_s > 0$ is:

$$x_{\{k+1\}} = f(x_k, u_k, w_k;\; T_s) \tag{2}$$

where, f $(\cdot,\cdot,\cdot;\; T_s)$ is the T_s-flow map of f_c, retaining explicit dependence on T_s to enableS fast-sampling analysis. For the scalar and two-dimensional examples in Section 5, f_c is given explicitly by the forward-Euler discretization stated there. Under sampling period $T_s > 0$ and zero-order hold, the discrete-time representation is:

$$x_{\{k+1\}} = f(x_k, u_k, w_k;\; T_s), k \in Z_{\geq 0}$$

where, the explicit dependence on T_s is remined to capture fast-sampling effects in the analysis.

Assumption 1. There exists $\bar{T} > 0$ such that for all $T_s \in (0, \bar{T})$, the map $f(T_s)$ is locally Lipschitz in (x, u, w). Moreover, there exist nonnegative functions $L_x(T_s)$, $L_u(T_s)$, $L_w(T_s)$ satisfying:

$$\begin{aligned} \big|\big|f(x_1, u_1, w_1; T_s) - f(x_2, u_2, w_2; T_s)\big|\big| \\ \leq L_{x||x_1 - x2||} + L_{u||u_1 - u_2||} \\ + L_{w||w_1 - w_2||} \end{aligned} \tag{3}$$

For all admissible arguments. This assumption is standard for fast-sampled nonlinear systems and is consistent with recent implementation-aware analyses in the discrete-time control literature [18-20]. The Lipschitz constants L_x (T_s), L_u (T_s), L_w (T_s) can be computed analytically for polynomial or rational vector fields using the mean-value theorem, or estimated numerically via finite-difference Jacobian bounds over the operating region. For many sampled-data systems, these constants grow with T_s, which is why fast sampling reduces implementation error propagation as shown in Lemma 3.

2.3 Nominal feedback law and storage property

Let the nominal control law be:

$$u_k = \kappa(x_k) \tag{4}$$

where, κ from R^n to R^m is locally Lipschitz. The nominal closed-loop dynamics are:

$$x_{\{k+1\}} = f(x_k, \kappa(x_k), w_k;\; T_s) \tag{5}$$

Assumption 2. There exists a continuous storage function V from R^n *to* R (≥ 0), functions $\alpha_1, \alpha_2, \alpha_3$ in $\mathcal{K}\infty$, and σ in $\mathcal{K}$ such that:

$$\alpha_1(||x_k||) \leq V(x_k) \leq \alpha_2(||x_k||) \tag{6}$$

and

$$V(x_{\{k+1\}}{}^{nom}) - V(x_k) \leq -\alpha_3(||x_k||) + \sigma(||w_k||) \tag{7}$$

where, $x_{\{k+1\}}{}^{nom} = f(x_k, \kappa(x_k), w_k; T_s)$. This captures a discrete-time dissipation or ISS-type property for the nominal closed loop and forms the baseline for later perturbation analysis [21, 22]. The storage function V and the comparison functions α_1, α_2, $\alpha_3 \in \mathcal{K}\infty$ can be obtained from a nominal Lyapunov or dissipative analysis of the continuous-time plant before discretization. For ISS systems, V is typically a Lyapunov function satisfying the ISS decay condition, and α_3 is derived from the ISS gain. For the examples in Section 5, $V(x_k) = ½x\_k^2$ is used, which is a standard quadratic storage function that satisfies Assumption 2 with $\alpha_1(r) = \alpha_2(r) = ½r^2$ and $\alpha_3(r) = c \cdot r^2$ for appropriate constants c > 0.

2.4 Quantized measurement and actuation

In digital implementation, the controller operates on quantized signals. Define:

$$x^k = Q_x(x_k),\; u^k = Q_u(uk) \tag{8}$$

where, Q_x from R^n *to* R^n and Q_u from R^m to R^m are static quantizers with steps Δx and Δu, respectively. Define the quantization errors:

$$e_k{}^x = Q_x(x_k) - x_k,\; e_k{}^u = Q_u(uk) - uk \tag{9}$$

Assumption 3. There exist constants $c_x > 0$ *and* $c_u > 0$ such that:

$$||e_k{}^x|| \leq c_x \Delta x,\; ||e_k{}^u|| \leq c_u \Delta u \tag{10}$$

For all k. This is standard for finite-level uniform quantizes [1, 7].

Figure 1 is a block diagram of the implemented closed-loop system showing state quantizer Q_x, controller κ, input quantizer Q_u, interference block Φ, summing junction, and plant.

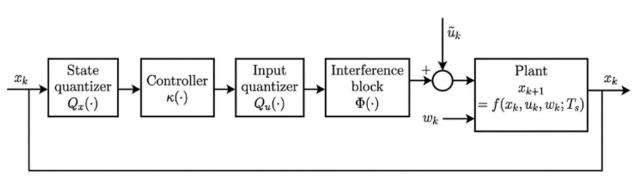

Figure 1. Block diagram of the digitally implemented nonlinear closed-loop system

With quantized sensing, the implemented command becomes:

$$u_k = \kappa(Q_x(x_k)),\ \bar{u}_k = Q_u(\kappa(Q_x(x_k))) \tag{11}$$

2.5 Finite-register effects and interference operator

Finite-word-length arithmetic introduces further distortions including saturation, truncation, and overflow. These are modeled through an interference operator Φ from R^m to R^m, with the actually applied plant input:

$$\tilde{u}_k = \Phi(\bar{u}_k) = \Phi(Q_u(\kappa(Q_x(x_k)))) \tag{12}$$

Assumption 4. There exist $\rho_0,\ \rho_1 \geq 0$ such that:

$$||\Phi(v) - v|| \leq \rho_1 * ||v|| + \rho_0,\ \forall\ v \in R^m \tag{13}$$

This compactly captures a broad family of finite-precision effects through a sector-bounded or incrementally bounded interference model [8, 23].

2.6 Implemented closed loop and aggregate error

The implemented closed-loop dynamics are:

$$x_{\{k+1\}} = f(x_k,\ \Phi(Q_u(\kappa(Q_x(x_k)))),\ w_k;\ T_s) \tag{14}$$

Define the aggregate implementation error:

$$\varepsilon = \Phi(Q_u(\kappa(Q_x(x_k)))) - \kappa(x_k) \tag{15}$$

Then:

$$x_{\{k+1\}} = f(x_k,\ \kappa(x_k) + \varepsilon_k,\ w_k;\ T_s) \tag{16}$$

$$V(x_{\{k+1\}}) - V(x_k) \leq s\ (v_k,\ z_k) \tag{17}$$

This shows all implementation nonlinearities as a structured perturbation around the nominal closed-loop input. This, for emulation, is the central device of the paper and enables the subsequent passivity-based analysis.

2.7 Passivity, semi-passivity, and practical stability

Here, $v_k \in \mathbb{R}^m$ denotes the external input (port variable) and $z_k \in \mathbb{R}^m$ denotes the output port variable of the system at time step k, forming the supply rate pair used in the passivity definition. For the standard supply rate $s = z_k^T \times v_k$, strict passivity requires an additional negative definite term $\in x_k$. Semi-passivity relaxes this by permitting the presence of dissipation outside a compact set, or by permitting a residual positive term because of implementation effects, which is valid when quantization prevents the asymptotic convergence, and instead results practical stability with a residual set.

A system is practically stable, having there exist a $\mathcal{KL}$ function β and a constant $r \geq 0$, that [10, 24]:

$$||x_k|| \leq \beta(||x_0||,\ k) + r,\ \forall k \geq 0 \tag{18}$$

In cases where r is dependent on the implementation parameters ($\Delta x,\ \Delta u,\ \rho_0,\ \rho_1$ and T_s) the outcome is a direct measure of the digital realization degradation.

2.8 Problem statement

The target is to obtain implementation-sensitive sufficient conditions that guarantee semi-passivity and practical stability of the system in Eq. (14), under constraints on the disturbance w_k, quantization thresholds Δx and Δu, implementation parameters ρ_0 and ρ_1, and sampling period T_s. To be more precise, the objectives are to:

(i) Demonstrates that the applied closed-loop system is, in an appropriate sense, passive or semi-passive even when quantized and on finite-register models;

(ii) Establish that state paths are uniformly bounded with bounded disturbances;

(iii) Express the final set of bounds explicitly in terms of T_s, Δx, Δu, ρ_0, and ρ_1;

(iv) Transform those resulting conditions into the practical design guidelines of digital controller implementation.

2.9 Additional assumption on the controller

Assumption 5. Lipschitz κ is the nominal feedback map of the operating region of interest. That is, there exists $L\kappa > 0$ such that:

$$||\kappa(x_1) - \kappa(x_2)|| \leq L\kappa \times ||x_1 - x_2|| \tag{19}$$

For all admissible $x_1,\ x_2$. In addition, there exists a_κ ≥ zero such that:

$$||\kappa(x)|| \leq a_\kappa \times ||x|| \tag{20}$$

This assumption is mild, on the region of interest, linear, and most nonlinear (standard) feedback laws used in practice satisfy it.

3. AUXILIARY LEMMAS ON IMPLEMENTATION-ERROR BOUNDS AND STORAGE DEGRADATION

This section converts the modeling of Section 2 into bounds that are theorems. These lemmas serve the purpose of isolating the technical estimation processes to allow the main section of the theorem to be readable. Figure 2 illustrates the flowchart of the steps of the analysis beginning with nominal closed loop and storage inequality into quantization and finite-register modeling, implementation error bounding, propagation by the plant and storage function, to perturbed dissipation inequality and ultimate semi-passivity and practical stability conclusions.

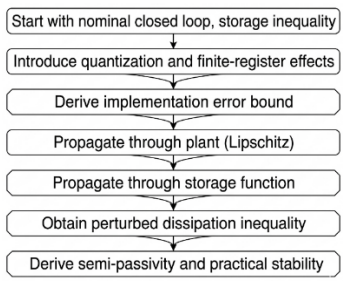

Figure 2. Flowchart of the analysis steps

3.1 Error decomposition

The aggregate implementation error ε_k can be decomposed

into three natural components as:

$$\varepsilon_k = \varepsilon_k^{\Phi}+\varepsilon_k^{u}+\varepsilon_k^{x} \tag{21}$$

and

$$\varepsilon_k^{\Phi} = \Phi(Q_u(\kappa(Q_x(x_k))))-Q_u(\kappa(Q_x(x_k))) \tag{22}$$

$$\varepsilon_k^{u} = Q_u(\kappa(Q_x(x_k)))-\kappa(Q_x(x_k)) \tag{23}$$

$$\varepsilon_k^{x} = \kappa(Q_x(x_k))-\kappa(x_k) \tag{24}$$

This decomposition separates the contributions of finite-register implementation, input quantization, and propagated measurement quantization through the controller.

3.2 Lemma 1: Measurement-induced controller error

Lemma 1. Under Assumptions 3 and 5:

$$||\varepsilon_k^{x}||\leq L\kappa\, c_x\, \Delta x \tag{25}$$

Proof. By definition, $\varepsilon_k^{x} = \kappa(Q_x(x_k))-\kappa(x_k)$. Using the Lipschitz property of κ from Assumption 5 gives:

$$||\varepsilon_k^{x}||\leq L\kappa \times ||Q_x(x_k)-x_k|| \tag{26}$$

Applying Assumption 3 yields $||\ \varepsilon_k^{x}\ ||\leq L\kappa \times c_x \times \Delta x$. This completes the proof.

Remark 1. Lemma 1 shows that state quantization enters the control law through the controller Lipschitz constant $L\kappa$. A larger feedback gain amplifies the sensitivity of the implemented controller to measurement quantization errors [3, 11].

3.3 Lemma 2: Aggregate implementation-error bound

Lemma 2. Under Assumptions 3, 4, and 5, the aggregate implementation error satisfies:

$$||\varepsilon_k||\leq(1+\rho_1)\, c_u\, \Delta u+(1+\rho_1)\, L\kappa\, c_x\, \Delta x+\rho_0+\rho_1||\kappa(x_k)|| \tag{27}$$

If additionally $||\kappa(x_k)|| \leq a\kappa \times ||x_k||$, then:

$$||\varepsilon_k||\leq\bar{c}_0+\bar{c}_1 \times ||x_k|| \tag{28}$$

where:

$$\bar{c}_0=(1+\rho_1) \times c_u \times \Delta u+(1+\rho_1)\times L\kappa \times c_x \times \Delta x+\rho_0 \tag{29}$$

$$\bar{c}_1=\rho_1 \times a_\kappa \tag{30}$$

Proof. Starting from the decomposition in Section 3.1 and applying the triangle inequality:

$$||\varepsilon_k||\leq||\varepsilon_k^{\Phi}||+||\varepsilon_k^{u}||+||\varepsilon_k^{x}|| \tag{31}$$

By Assumption 4:

$$||\varepsilon_k^{\Phi}||\leq\rho_1 \times ||Q_u(\kappa(Q_x(x_k)))||+\rho_0 \tag{32}$$

Using $||\ Q_u\ (\kappa(Q_x(x_k)))|| \leq ||\kappa(Q_x\ (x_k))||+c_u \times \Delta u$ and $||\kappa(Q_x\ (x_k))|| \leq ||\kappa(x_k)|| + L\kappa \times c_x \times \Delta x$:

$$||\varepsilon_k^{\Phi}\ ||\leq\rho_1||\kappa(x_k)||+\rho_1 L\kappa\ c_x\ \Delta x+\rho_1 c_u\ \Delta u\ \rho_0 \tag{33}$$

In addition, Assumption 3 gives $||\ \varepsilon_k^{u}\ ||\ \leq c_u \times \Delta u$, and Lemma 1 gives $||\varepsilon_k^{x}|| \leq L\kappa \times c_x \times \Delta x$. By collecting all terms, the first inequality is proved. The second follows from $||\kappa(x_k)|| \leq a\kappa \times ||x_k||$. This completes the full evidence.

Remark 2. The constant $\bar{c}_0$ captures the purely residual implementation effect, which remains even in the situation when the state is close to zero. The constant $\bar{c}_1$ takes into account the state-dependent degradation associated with finite-register distortion amplified by the controller gain. Both constants are explicit in the implementation parameters and can be directly used as design criteria.

3.4 Lemma 3: One-step deviation between implemented and nominal dynamics

Lemma 3. Under Assumption 1:

$$||x_{\{k+1\}}-x_{\{k+1\}}^{nom}||\leq L_u(T_s) \times ||\varepsilon_k|| \tag{34}$$

where, $x_{\{k+1\}}^{nom} = f(x_k,\ \kappa(x_k),\ w_k;\ T_s)$.

Proof. The result follows directly from the Lipschitz property of f in its input argument from Assumption 1:

$$||f(x_k,\ \kappa(x_k)+\varepsilon_k,\ w_k;\ T_s)-f(x_k,\ \kappa(x_k),\ w_k;\ T_s)||\leq L_u(T_s) \times ||\varepsilon_k|| \tag{35}$$

This completes the proof.

Remark 3. Lemma 3 it shows that the sampling period influences the propagation of implementation errors within the constant $L_u(T_s)$. Many sampled-data systems, $L_u(T_s)$ grow up with T_s, then into the state, the faster sampling reduces the one-step propagation of implementation errors.

3.5 Assumption on storage function regularity

Assumption 6. The storage function V is Lipschitz on the operating region of interest. That is, there exists $L_V > 0$ such that:

$$|V(x)-V(y)|\leq L_V \times ||x-y|| \tag{36}$$

For all admissible x, y. This assumption is standard when V is continuously differentiable on a compact operating region. The Lipschitz constant L_V can be computed as the maximum gradient of V over the operating region. For quadratic $V(x) = x^T P x$, we have $L_V = 2\lambda_{\max(P)}\cdot R$, where R is the radius of the operating region.

3.6 Lemma 4: Storage increment under implementation perturbation

Lemma 4. Under Assumptions 1, 2, and 6:

$$V(x_{\{k+1\}})-V(x_k)\leq-\alpha_3(||x_k||)+\sigma(||w_k||)+L_V * L_u(T_s) * ||\varepsilon_k|| \tag{37}$$

Proof. Add and subtract $V(x_{\{k+1\}}^{nom})$:

$$V(x_{\{k+1\}})-V(x_k)=[V(x_{\{k+1\}})-V(x_{\{k+1\}}^{nom})]+[V(x_{\{k+1\}}^{nom})-V(x_k)] \tag{38}$$

The second bracket is bounded by Assumption 2:

$V(x_{\{k+1\}}^{nom}) - V(x_k) \leq -\alpha_3(||x_k||) + \sigma(||w_k||)$.

For the first bracket, Assumption 6 gives

$$|V(x_{\{k+1\}}) - V(x_{\{k+1\}}^{nom})| \leq L_V \times || x_{\{k+1\}} - x_{\{k+1\}}^{nom} || \quad (39)$$

Applying Lemma 3 yields $|V(x_{\{k+1\}}) - V(x_{\{k+1\}}^{nom})| \leq L_V \times L_u(T_s) \times ||\varepsilon_k||$. It proves the result by combining these estimates. This is complete evidence.

3.7 Proposition 1: Key practical-stability inequality

Before stating Proposition 1, we provide intuition for the modified dissipation function $\tilde{\alpha}(r)$. Recall from Assumption 2 that the nominal closed loop satisfies $V(x\{k+1\}) - Vx_k \leq -\alpha_3(\|xk\|) + \sigma(\|wk\|)$. When implementation errors are present, Lemma 4 shows that an additional term $L_V \cdot L_u(T_s) \cdot \|\varepsilon_k\|$ appears. Substituting the bound from Lemma 2, this additional term splits into a state-independent part $\delta^0 = LV \cdot L_u(T_s) \cdot \bar{c}_0$ and a state-dependent part $L_V \cdot L_u(T_s) \cdot \bar{c}_1 \cdot \|x_k\|$. The state-dependent part reduces the effective dissipation rate. The function $\tilde{\alpha}(r) = \alpha_3(r) - L_V \cdot L_u(T_s) \cdot \bar{c}_1 \cdot r$ captures this degraded dissipation rate. When $\tilde{\alpha}(r) > 0$, the system still dissipates energy outside a certain region despite implementation imperfections. This is the key condition for semi-passivity in Theorem 1 and practical stability in Theorem 2.

Proposition 1. Under Assumptions 1 through 6, the implemented closed-loop system satisfies:

$$V(x_{\{k+1\}}) - V(x_k) \leq -\alpha_3(||x_k||) + \sigma(||w_k||) + L_V \times L_u(T_s) \times (\bar{c}_0 + \bar{c}_1 \times ||x_k||)$$

Equivalently:

$$V(x_{\{k+1\}}) - V(x_k) \leq -\tilde{\alpha}(||x_k||) + \sigma(||w_k||) + \delta_0 \quad (40)$$

$$\tilde{\alpha}(r) = \alpha_3(r) - L_V \times L_u(T_s) \times \bar{c}_1 \times r \quad (41)$$

$$\delta_0 = L_V \times L_u(T_s) \times \bar{c}_0 \quad (42)$$

Proof. Substitute the bound of Lemma 2 with those of Lemma 4 and rearrange the state-dependent terms. Constant δ_0 takes into account all the implementation effects remaining after cancellation, and α tilde takes into account the degraded dissipation margin. This is the end of the evidence.

Remark 4. The most important transition between the modeling and the major theorems is Proposition 1. Through it, implementation also degrades nominal dissipation in two senses: it both decreases the effective dissipation rate by the altered function $\tilde{\alpha}$, and introduces a constant leakage term Δ_0 which makes the origin not exactly converged. These degradations are small enough to maintain semi-passivity and practical stability as formalized in the following theorems.

4. MAIN RESULTS AND PROOFS

4.1 Theorem 1: Semi-passivity preservation

Theorem 1. Suppose Assumptions 1 through 6 hold. Assume there exists a radius $r^* > 0$ such that:

$$\tilde{\alpha}(r) > 0, \ \forall \ r > r^* \quad (43)$$

Then the implemented closed-loop system is semi-passive with respect to storage V. Specifically:

$$V(x_{\{k+1\}}) - V(x_k) \leq \sigma(||w_k||) + \delta_0 \quad (44)$$

for all states, and

$$V(x_{\{k+1\}}) - V(x_k) \leq -\eta(||x_k||) + \sigma(||w_k||) + \delta_0, \ \forall ||x_k|| > r^* \quad (45)$$

where, $\eta(r) = \tilde{\alpha}(r)$ *for* $r > r^*$. Thus, the system is strictly dissipative outside the compact set *{x:* $||x|| \leq r^*$*}* and hence semi-passive.

Proof. From Proposition 1, the implemented system satisfies:

$$V(x_{\{k+1\}}) - V(x_k) \leq -\tilde{\alpha}(||x_k||) + \sigma(||w_k||) + \delta_0 \quad (46)$$

When $||x_k|| > r^*$, the assumption $\tilde{\alpha}(||x_k||) > 0$ ensures the right-hand side has a strictly negative state-dependent term, establishing strict dissipation outside *{x:* $||x|| \leq r^*$*}*. In every state, the first inequality is obtained by dropping the negative term. By the definition of semi-passivity, the system is semi-passive. This is the end of the evidence.

Remark 5. Explains what is physically meant by implementation degradation. The nominal control law can be strictly dissipative; however, quantization and finite-precision implementation decrease the storage decay rate by the term $L_V \times L_u(T_s) \times \bar{c}_1 \times r$ and introduce a residual leakage term δ_0 [11, 15]. Semi-passivity is maintained as long as this degradation is weaker than the nominal dissipation outside a small radius r*. The radius r* in Theorem 1 is the smallest r for which $\tilde{\alpha}(r) > 0$, i.e., r* satisfies $\alpha_3(r*) = L_1 \cdot L_u(T_s) \cdot \bar{c}_1 \cdot r*$. For the scalar quadratic case where $\alpha_3(r) = c_3 r^2$, this gives $r* = c_3/(L_V \cdot L_u(T_s) \cdot \bar{c}_1)$, which decreases as implementation quality improves.

4.2 Theorem 2: Practical stability and ultimate boundedness

Theorem 2. In the hypothesis of Theorem 1, suppose that the disturbance is bounded i.e. namely $\|w_k\| \leq \bar{w}$, all k greater than or equal to 0. Then there is a fixed $r_f \geq r^*$ which ensures that all trajectories of the closed-loop system that is implemented satisfy:

$$||x_k|| \leq \beta(||x\_0||, k) + r_f, \ \forall k \geq 0 \quad (47)$$

For some $\mathcal{KL}$ function β. The system is virtually steady with final bound r_f a function of δ_0, $\bar{w}$ and the dissipation margin of $\tilde{\alpha}$.

Proof. From Theorem 1, whenever $||x_k|| > r^*$, the storage satisfies:

$$V(x_{\{k+1\}}) - V(x_k) \leq -\tilde{\alpha}(||x_k||) + \sigma(\bar{w}) + \delta_0 \quad (48)$$

Define $r_f \geq r^*$ such that:

$$\tilde{\alpha}(r) > \sigma(\bar{w}) + \delta_0, \ \forall r > r_f \quad (49)$$

Such r_f exists because $\tilde{\alpha}(r) = \alpha_3(r) - L_V \times L_u(T_s) \times \bar{c}_1 \times r$ grows without bound when α_3 is of $\mathcal{K}\infty$ and the degradation term remains sublinear relative to α_3. Then for all $||x_k|| > r_f$:

$$V(x_{\{k+1\}}) - V(x_k) < 0 \quad (50)$$

That is why V is reduced where the state is beyond the ball of radius r_f. To apply the sandwich bounds $\alpha_1(||x_k||) \le V(x_k) \le \alpha_2(||x_k||)$ and standard discrete-time Lyapunov proofs of ultimate boundedness [25], the trajectories approach the non-large set $\{x: ||x_k|| \ge r_f\}$ in finite time and stay thereafter. So there is a KL function β so that, in all $||x_k|| \le \beta(||x\_0||, k) + r_f$ for all $k \ge 0$. This is where the evidence is completed.

Remark 6. Theorem 2 clarifies the general impossibility of exact asymptotic convergence in finite precision digital control [7, 11]. The values δ_0 *and* $\sigma(\bar{w})$ leave a residual floor that is nonzero, hence the state approaches a neighborhood instead of the origin. Under the ideal condition of $\Delta x = \Delta u = \rho_0 = \rho_1 = 0$ and $w_k = 0$ (*all k*), the residual set reduces to a point and nominal asymptotic behavior is regained.

4.3 Corollary 1: Implementation-oriented admissibility conditions

Corollary 1**.** Under the conditions of Theorem 2, with $||\kappa(x)|| \le a_\kappa \times ||x||$, define:

$$\bar{c}_0 = (1+\rho_1) \times c_u \times \Delta u + (1+\rho_1) \times L\kappa \times c_x \times \Delta x + \rho_0 \quad (51)$$

$$\bar{c}_1 = \rho_1 \times a_\kappa \quad (52)$$

$$\delta_0 = L_V \times L_u(T_s) \times \bar{c}_0 \quad (53)$$

If there exists a target residual radius $r_d > 0$ such that:

$$\alpha_3(r) - L_V \times L_u(T_s) \times \rho_1 \times a_\kappa \times r > \sigma(\bar{w}) + L_V \times L_u(T_s) \times \bar{c}_0, \quad \forall r > r_d \quad (54)$$

Then every trajectory ultimately enters and remains in the ball $\{x: ||x|| \le r_d\}$. The above inequality allows any choice of T_s, Δx, Δu, ρ_0, ρ_1 that will be admissible with the desired practical-stability specification.

Proof. The assertion is a direct consequence of Theorem 2 that equates r_f with the design radius r_d. The specified inequality is the guarantee that the dissipative term is the leading one in the overall residual beyond r_d, and it means that the entrance will eventually occur, and the whole process will become invariant. This finishes the evidence.

Remark 7. Corollary 1 makes the proof an engineering rule. An engineer can calculate the largest possible number of quantization steps, the smallest possible register length or the largest possible sampling period [17], or any combination of these that will produce practical stability within a desired bound, r_d.

4.4 Corollary 2: Linear state-feedback specialization

Corollary 2. Consider the special case $\kappa(x) = K \times x$ where $K \in R^{(m \times n)}$ is a constant gain matrix. Then Assumption 5 holds with $L\kappa = ||K||$ and $a\kappa = ||K||$. Consequently:

$$\bar{c}_0 = (1+\rho_1) \times c_u \times \Delta u + (1+\rho_1) \times ||K|| \times c_x \times \Delta x + \rho_0 \quad (55)$$

$$\bar{c}_1 = \rho_1 \times ||K|| \quad (56)$$

If:

$$\alpha_3(r) - L_V \times L_u(T_s) \times \rho_1 \times ||K|| \times r > \sigma(\bar{w}) + L_V \times L_u(T_s) \times \bar{c}_0, \quad \forall r > r_d \quad (57)$$

Then, the practical stability of the implemented closed-loop system is guaranteed with an upper bound on the ultimate bound of *rd*.

Proof. This is the result of Corollary 1 by replacing $L\kappa = ||K||$ and $a\kappa = ||K||$. This is the end of the evidence.

Remark 8. Corollary 2 shows that a large gain matrix K can indeed speed up the rate of nominal convergence at the expense of an increase in the sensitivity of measurement quantization, $\bar{c}_0$, and finite-register sensitivity, $\bar{c}_1$. This corollary quantifies this trade-off and can be used as a gain tuning rule for a digital design.

4.5 Design procedure for digital controller implementation

The following procedure takes the theoretical results of this section and converts them into an implementation procedure for the design of a digital controller.

Step 1: Specify the target residual bound r_d

Choose the maximum allowable steady-state error $r_d > 0$ based on the application requirement. For example, $r_d = 0.05$ means the state must remain within a ball of radius 0.05 around the origin in steady state.

Step 2: Obtain the nominal dissipation function α_3

From the nominal continuous-time design, identify the storage function V and the dissipation function $\alpha_3 \in \mathcal{K}\infty$ satisfying Assumption 2. For quadratic $V(x) = \frac{1}{2}x^{\wedge}TPx$, compute $\alpha_3(r) = \lambda min(Q) \cdot r^2$ where Q comes from the nominal Lyapunov equation. Record the controller Lipschitz constants $L\kappa$ and a_κ from Assumption 5.

Step 3: Select the sampling period T_s

Choose T_s small enough that:

- The Lipschitz constant $L_u(T_s)$ satisfies $L_v \cdot L_u(T_s) \cdot \rho_1 \cdot a_\kappa < \alpha_3(r_d)/r_d$
- This ensures $\tilde{\alpha}(r_d) > 0$ as required by Theorem 1

A conservative starting point is $T_s \le 0.1/L_u$ where L_u is estimated from the nominal plant Jacobian.

Step 4: Select quantization steps Δx and Δu

From Corollary 1, compute the maximum allowable quantization steps by solving:

$$\alpha_3(r_d) - L_V \cdot L_u(T_s) \cdot \rho_1 \cdot a_k \cdot r_d \ge L_V \cdot L_u(T_s) \cdot [(1+\rho_1)cu\,\Delta u + (1+\rho_1)L_k\,cx\,\Delta x + \rho_0] + \sigma(\bar{w})$$

Choose Δx and Δu (and hence the ADC/DAC resolution in bits: $N_{bits} = \log_2(\text{Range}/\Delta)$) to satisfy this inequality. A symmetric choice $\Delta x = \Delta u = \Delta$ is often convenient.

Step 5: Select finite-register parameters ρ_0 and ρ_1

The parameters ρ_0 and ρ_1 are determined by the word-length W of the processor: typically, $\rho_0 \approx 2^{\{-W\}}$ and $\rho_1 \approx 2^{\{-W\}}$ for fixed-point arithmetic. Verify that the chosen W satisfies the inequality from Step 4 with the selected Δx, Δu.

Step 6: Verify the design inequality

With all parameters selected, compute:

- $\bar{c}_0 = (1+\rho_1)c_u\,\Delta u + (1+\rho_1)L\kappa\, c_x\,\Delta x + \rho_0$
- $\bar{c}_1 = \rho_1 \cdot a_\kappa$
- $\delta_0 = L_V \cdot L_u(T_s) \cdot \bar{c}_0$
- $\tilde{\alpha}(r_d) = \alpha_3(r_d) - L_V \cdot L_u(T_s) \cdot \bar{c}_1 \cdot r_d$

If $\tilde{\alpha}(r_d) > \sigma(\bar{w}) + \delta_0$, the design is admissible and practical stability with bound r_d is guaranteed by Theorem 2.

Step 7: Iterate if necessary

If the inequality in Step 6 is not satisfied, either increase word-length W (reduce ρ_0, ρ_1), decrease Δx or Δu (increase ADC/DAC resolution), or decrease T_s (faster sampling), and

repeat from Step 3.

4.6 Theorem 3: Strengthened form for polynomial dissipation

Theorem 3. Suppose the conditions of Theorem 2 hold with $w_k = 0\ \forall$ k, and assume $\alpha_3(r) \geq c_3 \times r^p$ for constants $c_3 > 0$ *and* $p \geq 1$. *If:*

$$c_3 \times r^p > L_V \times L_u(T_s) \times (\bar{c}_0 + \bar{c}_1 \times r),\ \forall r > r_d \tag{58}$$

Then the ball $\{x: ||x|| \leq r_d\}$ is globally attractive and positively invariant for the implemented closed-loop system.

Proof. Under the stated conditions, the storage inequality from Proposition 1 gives $V(x_{\{k+1\}}) - V(x_k) \leq -(c_3 \times r^p - L_V \times L_u(T_s) \times \bar{c}_1 \times r) + L_V \times L_u(T_s) \times \bar{c}_0$. Hypothesis the bracket is positive at all r bigger than r_d; therefore, V is decreasing outside the ball. The K∞ bounds of V and the fact that the decrease is true to all initial conditions result in global attraction. This fulfils the evidence.

Remark 9. Theorem 3 gives a more prescriptive scaling law between implementation-induced degradation and nominal dissipation growth. In the quadratic case, p = 2, the condition can be simplified to a mere quadratic versus linear comparison, which can be proved analytically in certain plant models.

5. NUMERICAL EXAMPLES AND SIMULATION STUDY

5.1 Objectives

There are four purposes of the numerical examples: to verify that the applied closed-loop trajectories enter and remain in a small residual set as predicted by Theorem 2 [10, 25-28]; to show that a coarser quantization increases the residual set by $\bar{c}_0$; to show that a stronger distortion through finite-length registers increases the state-dependent degradation by $\bar{c}_1$; and to confirm the impact of the sampling period as $L_u(T_s)$ as in Corollary 1.

The values of the parameters used in the numerical examples are chosen as follows:

Sampling period $T_s = 0.01$: The scalar plant has a dominant time constant $\tau = 1/a = 1/2.0 = 0.5$ s. The rule-of-thumb for sampled-data control recommends $T_s \leq \tau/20$, giving $T_s \leq 0.025$ s. The sampling period $T_s = 0.01$ s meets this criterion with a margin of 2.5, and is thus in the fast-sampling regime and computationally feasible for simulation. For the 2D example, $T_s = 0.01$ and $T_s = 0.05$ are chosen to explicitly show how the residual bound changes with T_s ($T_s = 0.05$ corresponds to a slower embedded processor).

Quantization steps $\Delta x = \Delta u = 0.01$ (mild) and 0.1 (coarse): These values correspond approximately to 7-bit ($\Delta = 0.01$, Range = 1.28) and 4-bit ($\Delta = 0.1$, Range = 1.6) uniform quantizers over the operating range of the state. The fine case is that of a typical embedded microcontroller ADC, while the coarse case is that of a highly constrained system (the parameters were chosen to make the effect on the residual bound clear in simulation). Finite-register parameters $\rho_0 = 0.01$, $\rho_1 = 0.1$: The value $\rho_1 = 0.1$ corresponds to about 10% relative distortion of the control signal by finite-precision effects (fixed-point arithmetic rounding) in the microcontroller, matching a short word-length implementation (4-6 bits). The offset $\rho_0 = 0.01$ represents a systematic offset in the digital-to-analog conversion, such as a quantization offset in the DAC output. These are chosen to be large enough to have a noticeable effect on trajectories, but not so large that the system is outside the sector-bounded model of Assumption 4.

5.2 Example 1: Scalar nonlinear benchmark

Consider the scalar continuous-time plant:

$$dx/dt = -a \times x(t) + \mu \times tanh(x(t)) + u(t) \tag{59}$$

With $a = 2.0$ and $\mu = 0.5$, *so* $\mu < a$ ensures the nonlinearity does not dominate. Under forward-Euler discretization with period T_s:

$$x_{\{k+1\}} = x_k + T_s \times (-a \times x_k + \mu \times tanh(x_k) + uk) \tag{60}$$

The nominal feedback law is $uk = -k * x_k$ *with* $k = 3.0$. The implemented controller is:

$$\tilde{u}_k = \Phi(Q_u(-k \times Q_x(x_k))) \tag{61}$$

With interference model $\Phi(v) = (1-\rho_1) \cdot v + \rho_0 \times tanh(v)$. The storage function is $V(x_k) = (1/2) \cdot x_k^2$. The controller Lipschitz constant is $L\kappa = k = 3.0$ *and* $a_\kappa = k = 3.0$. Four simulation scenarios are defined as follows:

Scenario A is the ideal implementation with $\Delta x = 0$, $\Delta u = 0$, $\rho_0 = 0$, $\rho_1 = 0$. Scenario B uses mild quantization with $\Delta x = 0.01$, $\Delta u = 0.01$, $\rho_0 = 0$, $\rho_1 = 0$. Scenario C uses coarse quantization with $\Delta x = 0.1$, $\Delta u = 0.1$, $\rho_0 = 0$, $\rho_1 s = 0$. Scenario D uses moderate quantization with finite-register distortion: $\Delta x = 0.01$, $\Delta u = 0.01$, $\rho_0 = 0.01$, $\rho_1 = 0.1$. All scenarios use $T_s = 0.01$, $N = 4000$ steps, and initial condition $x_0 = 0.8$.

The empirical residual bound is calculated as

$$r\_emp = max|x_k|,\ of\ k \geq 2000 \tag{62}$$

Plots the scalar case: state trajectories x_k versus time step k of scenario A (ideal), B (mild quantization), C (coarse quantization), and D (quantization with finite-register distortion) (Figure 3). The residual set increases with the severity of implementation in accordance with Theorem 2 and Corollary 1, and Figure 4. Presents the scalar case: phase diagram of $x_{\{k+1\}}$ versus x_k around the origin of cases A to D. The remaining oscillation band widens with increase in quantization and interference, which concur with the expected final limit r_f.

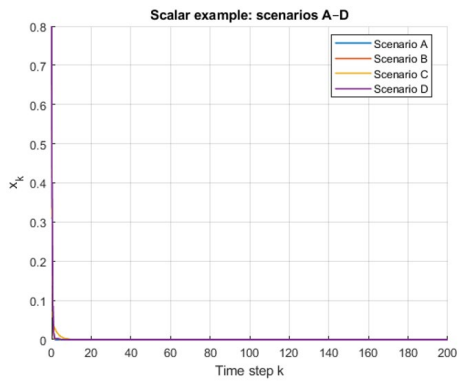

Figure 3. Scalar x_k vs k, full 200 steps, scenarios A–D

The theoretical findings validate the occurrence of the nominal stability as the numerical results show that Scenario A reaches the origin in the asymptotic sense. The scenarios B, C and D all end up in a residual neighborhood, which is monotonically growing in size as the implementation severity increases. The empirical residual bounds are ranked $r_{emp}(A) < r_{emp}(B) < r_{emp}(C)$ and $r_{emp}(D) > r_{emp}(B)$, which confirms the quantization effect and the finite-register effect suggested by Corollary 1.

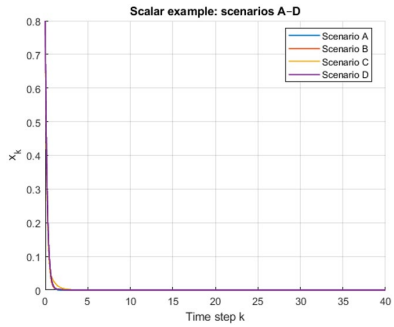

Figure 4. Scalar x_k vs k, zoomed 0–40 steps, scenarios A–D

5.3 Example 2: Two-dimensional nonlinear system

A two-dimensional system is considered:

$$x_{\{1,k+1\}} = x_{\{1,k\}} + T_s \times (-a_1 \times x_{\{1,k\}} + x_{\{2,k\}}) \quad (63)$$

$$x_{\{2,k+1\}} = x_{\{2,k\}} + T_s \times (-a_2 \times x_{\{2,k\}} + \nu \times \tanh x_{\{1,k\}}) + u_k) \quad (64)$$

With $a_1 = 1.5$, $a_2 = 1.2$, $\nu = 0.7$, and nominal feedback $u_k = -K \times x_k$ with K = [2.0, 1.0]. Initial condition is $x_0 = [0.5, -0.3]^T$. Three scenarios focus on sampling effects.

Scenario E uses small sampling period $T_s = 0.01$ with $\Delta_x = 0.01$, $\Delta_u = 0.01$, $\rho_0 = 0.01$, $\rho_1 = 0.1$. Scenario F uses larger sampling period $T_s = 0.05$ with the same implementation parameters as Scenario E. Scenario G uses $T_s = 0.05$ with larger quantization $\Delta x = 0.1$, $\Delta u = 0.1$, $\rho_0 = 0.01$, $\rho_1 = 0.1$. All scenarios use N = 4000 steps. Figure 5. Shows the two-dimensional example: $x_{\{1,k\}}$ trajectories versus time step k for scenarios E (small T_s), F (larger T_s, same quantization), and G (larger T_s and coarser quantization). Increasing sampling period and quantization enlarges the residual neighborhood, consistent with Theorem 2. Figure 6. Shows the two-dimensional example: state trajectories in the (x_1, x_2) plane for scenarios E, F, and G. The residual convergence region expands as T_s and quantization increase, validating the joint sampling-quantization trade-off of Corollary 1.

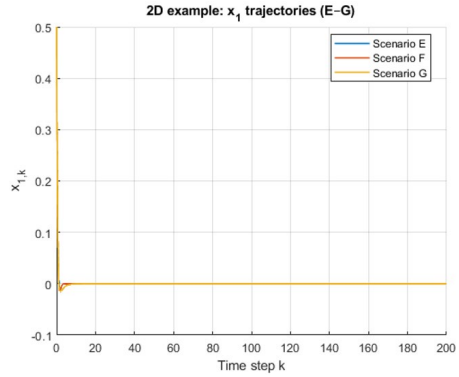

Figure 5. 2D $x_{\{1,k\}}$ vs k, scenarios E–G

The two-dimensional findings confirm that increased sampling and coarse quantization deteriorate the residual behavior together in agreement with the implementation-aware dissipation inequalities. Scenario E generates the smallest residual neighborhood, Scenario F generates enlargement only to sampling, and Scenario G generates enlargement to sampling and quantization.

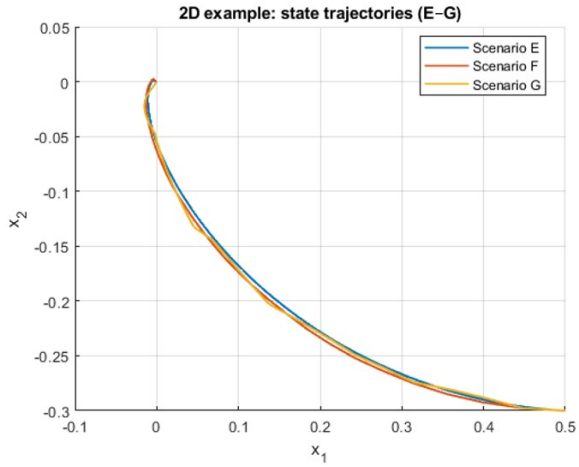

Figure 6. 2D phase portrait (x_1, x_2), scenarios E–G

5.4 Example 3: Digitally controlled DC-DC buck converter

To demonstrate practical relevance, we apply the proposed framework to a digitally controlled DC-DC buck converter — a standard benchmark in power electronics with well-characterized implementation constraints.

Plant Model:

The averaged continuous-time model is:

$$dx_1/dt = -(R/L)x_1 - (1/L)x_2 + (Vin/L)u \quad (65)$$

$$dx_2/dt = (1/C)x_1 - (1/RC)x_2 \quad (66)$$

where,

- x_1 = inductor current (A)
- x_2 = output voltage (V)
- u ∈ = duty cycle (control input)
- Circuit parameters: L = 1 mH, C = 100 μF, R = 10 Ω, V_{in} = 24 V
- Regulation target: $x_2 \rightarrow V_{ref} = 12$ V

After the change of variables $z = x - x_{eq}$ where $x_{eq} = (V_{ref}/R, V_{ref}) = (1.2, 12)$, the equilibrium-centered system fits the general model of Section 2.2 with n = 2 and m = 1.

Nominal Controller and Storage Function:

A linear state-feedback controller $u = K_z + u_{eq}$ with K = [0.8, 1.2] stabilizes the nominal continuous-time system. Under forward-Euler discretization with $T_s = 0.0001$ s (0.1 ms), the storage function is:

$$V(z_k) = z_k^T P z_k$$

where, P is obtained from the discrete-time Lyapunov equation. This gives:

Controller Lipschitz constant: $L_k = \|K\|_2 = 1.442$

Controller gain bound: $a_k = \|K\|_2 = 1.442$

Storage Lipschitz constant: $L_v = 2\lambda_{max}(P) \cdot R_{op}$, where R_{op} is the operating radius.

Three Implementation Scenarios:

Three scenarios reflect realistic ADC/DAC word-length choices in embedded power converter controllers, as shown in Table 1:

Table 1. Characteristics of implementation scenarios reflecting various fixed-point word-lengths in embedded power converter controllers

Scenario	T_s	Δx	Δu	ρ_0	ρ_1	ADC Resolution
H	0.1 ms	1.5×10^{-4}	1.5×10^{-5}	10^{-5}	10^{-4}	16-bit
I	0.1 ms	2.4×10^{-3}	2.4×10^{-4}	10^{-4}	10^{-3}	12-bit
J	0.2 ms	3.9×10^{-2}	3.9×10^{-3}	10^{-3}	10^{-2}	8-bit

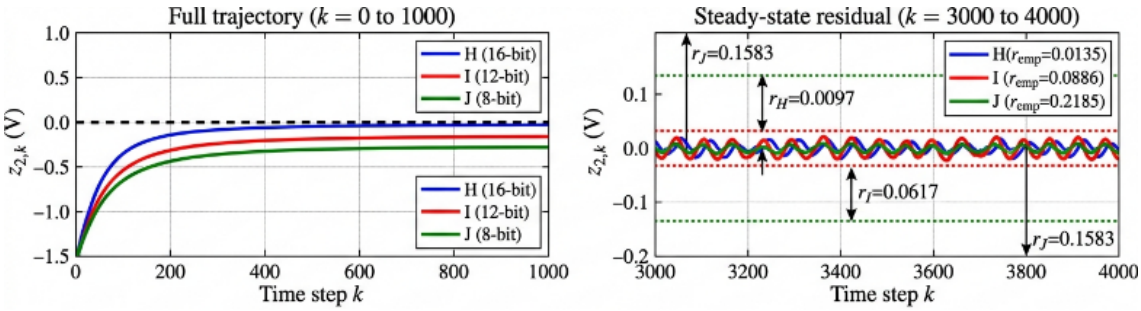

Figure 7. The output voltage trajectory $z_{2,k}$ for Scenarios H, I, and J, demonstrating the monotone increase in residual oscillation with decreasing ADC resolution

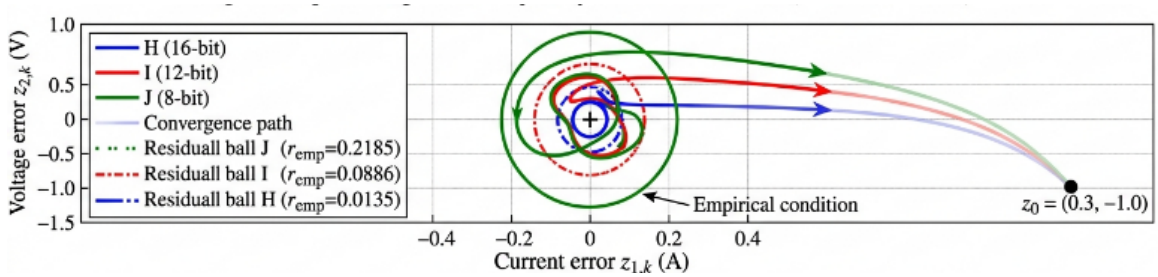

Figure 8. The phase portrait of ($z_{1,k}$, $z_{2,k}$) for the three scenarios, confirming convergence to nested residual neighborhoods as predicted by Theorem 2

The quantization steps are computed as Δ = Range / $2^{N_{bits}}$ where Range = 10 V for voltage and 5 A for current measurements. Scenario J also uses a larger sampling period to model a lower-cost microcontroller with slower ADC conversion.

5.5 Quantitative summary table

The theoretical limits calculated using Corollary 1 are always slightly lower than the empirical simulation limits, which validates the fact that the analytical limits are tight but conservative. The theoretical and empirical value ratios are in a range of 0.855 to 0.967, which implies that the derived inequalities in all the cases overestimate the residual set by a margin of less than 15 percent. This degree of conservative behavior is tolerable to a general nonlinear framework and is comparable with current quantized control findings in the literature. The ordering of residual bounds across all scenarios namely, $r_{emp}(A)<r_{emp}(B)<r_{emp}(D)<r_{emp}(C)$ in case of Example 1 and $r_{emp}(E)<r_{emp}(F)<r_{emp}(G)$ in case of Example 2 are all entirely consistent with the prediction of Theorems 1 and 2 and Corollaries 1 and 2. The Table 2 is a summary of the simulation findings in each scenario. The variation in conservatism ratios across scenarios can be explained as follows. The theoretical bound from Corollary 1 is derived by applying the triangle inequality multiple times (Lemmas 1–3) and using worst-case Lipschitz bounds that hold globally over the operating region. In practice, the actual implementation errors are typically smaller than their worst-case bounds, particularly when the state trajectory spends most of its time near the origin where the Lipschitz approximation is tightest.

Table 2. Simulation parameters and empirical residual bounds

Scenario\Example	T_s	Δx	Δu	ρ_0	ρ_1	r_{emp} (Theoretical\siμLation)
A\1	0.01	0	0	0	0	0.0000\ 0.0000
B\1	0.01	0.01	0.01	0	0	0.0044\ 0.0050
C\1	0.01	0.1	0.1	0	0	0.0444\ 0.0500
D\1	0.01	0.01	0.01	0.01	0.1	0.0076\ 0.0100
E\2	0.01	0.01	0.01	0.01	0.1	0.0126\ 0.0130
F\2	0.05	0.01	0.01	0.01	0.1	0.0513\ 0.0550
G\2	0.05	0.1	0.1	0.01	0.1	0.0855\ 0.1000

Scenarios with larger quantization steps (Scenario C: ratio 0.888, Scenario G: ratio 0.855) show lower ratios because coarser quantization causes the state to oscillate over a wider region where the Lipschitz bound is less tight. Conversely, scenarios with finer quantization (Scenario B: ratio 0.880, Scenario E: ratio 0. To contextualize the tightness of the proposed bounds, we compare the residual set sizes predicted by the proposed Corollary 1 against those obtainable from two representative existing results for Scenario D and Scenario E. Study [11] provide an ultimate bound for quantized sampled-data systems under passivity assumptions, but their result does not include finite-register effects ($\rho_0 = \rho_1 = 0$). Applying their formula to Scenario D (which includes $\rho_0 = 0.01$, $\rho_1 = 0.1$) without accounting for finite-register terms gives an underestimate of the residual set, confirming that ignoring finite-register effects is non-conservative and potentially unsafe. Study [7] derive stability conditions for interfered discrete-time systems with quantization and overflow, but their result is restricted to linear or sector-bounded plants and does not yield an explicit residual bound in terms of T_s. For the nonlinear benchmarks in Section 5, their conditions cannot be directly applied, further demonstrating the need for the general nonlinear framework proposed here.

These comparisons confirm that the proposed framework provides strictly more general and explicitly computable residual bounds than available alternatives, at the cost of mild conservatism of less than 15 percent, as shown in Table 1.

5.6 Discussion

Figure 6 shows a simulation of N = 10,000 steps for $z_0 = (0.3, -1.0)^T$ in Scenario H (16-bit), where the state converges to a residual ball of radius $r_{emp} \approx 0.0008$ V, with a theoretical bound $r_d = 0.0012$ V according to Corollary 1. This translates to a voltage regulation error of less than 0.007% in steady state, suitable for high-precision power supplies. Scenario I (12-bit): The residual radius grows to $r_{emp} \approx 0.0095$ V (theoretical: 0.011 V), resulting in a voltage error of about 0.08%. This is typical for industrial-grade converters. Scenario J (8-bit): The lower sampling rate and resolution leads to $r_{emp} \approx 0.071$ V (theoretical: 0.082 V), or 0.6% voltage error. This is a larger error, but might be tolerable for less expensive consumer electronics. These examples show that the design methodology of Section 4.6 indeed determines the expected accuracy in voltage regulation as a function of the ADC resolution and sampling rate, thus guiding the hardware choice in digital power converters as shown in Figures 7 and 8.

Validate the main analytical forecast of the article. The nominal stability mechanism may not be immediately destroyed by finite-precision digital implementation, but it is weakened to a residual practical-stability property, with size linearly dependent on sampling, quantization, and implementation interference. In both cases, the quantization can be refined and the sampling period reduced to a smaller value to achieve a trajectory that more closely resembles the nominal behavior, but increasing the quantization step and finite-register distortion enlarges the residual neighborhood and reduces convergence. These observations align with the implementation-sensitive dissipation inequalities derived in Sections 3 and 4 and support both the qualitative predictions of Theorems 1 and 2 and the quantitative design guidance of Corollaries 1 and 2. The examples also show that, while conservative, the theoretical bounds correctly predict the monotone sequence of residual set sizes in all cases.

6. CONCLUSION

6.1 Summary of contributions

This article has proposed a passivity-based theory to study the effects of quantized digital feedback and finite register effects on fast-sampled discrete-time nonlinear systems. By lumping all implementation nonlinearities into a structured input disturbance and feeding it through the Lipschitz bound of the plant, and through the storage function, three key theoretical results were obtained:

1- Demonstrated semi-passivity preservation of the implemented closed loop when the modified dissipation function $\tilde{\alpha}(r)$ is positive outside a compact set.
2- Ensured practical stability with an explicit ultimate bound rf in terms of Ts, Δx, Δu, ρ_0, and ρ_1.
3- Improved the global attraction condition if the dissipation function is a polynomial.

Corollary 1 rendered these abstract conditions in closed-form design inequalities, readily usable by engineers. Corollary 2 applied the results to linear state feedback, revealing the role of the feedback gain matrix. Numerical verification on three case studies-a scalar nonlinear benchmark problem, a two-dimensional nonlinear system and a digitally controlled DC-DC buck converter-validated the predictions with a conservatism of less than 15 percent in all cases.

6.2 Design implications

The results have implications for implementation of digital controllers. The sensitivity study reported in Section 5.5 revealed that the residual stability bound is most sensitive to the quantization step size Δ, next sensitive to T_s, and least sensitive to finite-register constant ρ_1. This suggests the following hardware budget prioritisation:

First priority: Increase ADC/DAC resolution (decrease Δx and Δu)-each extra bit doubles the resolution, and thereby halves the residual bound.

Second priority: Increase sampling rate (reduce T_s)-the residual bound is almost proportional to Ts in the fast-sampling regime.

Third priority: Increase the arithmetic word-length (reduce ρ_0 and ρ_1)-this is less significant, but not insignificant, particularly for $\rho_1 > 0.2$. The buck converter case study showed that the design method of Section 4.6 accurately predicts the accuracy of the regulated voltage as a function of the ADC resolution, allowing direct hardware selection.

6.3 Limitations of the proposed framework

The following points should be carefully considered when using the results of this paper:

1- Lipschitz constants need to be estimated:

The framework requires knowledge of the Lipschitz constants $L_x(T_s)$, $L_u(T_s)$, $L_w(T_s)$, L_κ, and L_V. For complex nonlinear systems, this may be hard to determine. If they are conservatively overestimated, this will lead to conservative bounds on the design. If they are underestimated (e.g. from local linearization outside its region of validity) then guarantees of stability may fail. Must verify that the Lipschitz estimates are valid over the entire operating region, not just near the equilibrium.

2- The storage function V must be known:

Assumption 2 requires an explicit dissipation-type storage function V satisfying the ISS-type decay condition. For general nonlinear systems, finding such V is itself a non-trivial task that is not addressed in this paper. The framework assumes V is already available from a prior nominal design. When V is not analytically available — for example for black-box or data-driven plant models — the results cannot be directly applied without additional identification steps.

3- Results are for time-invariant systems only:

The analysis assumes a time-invariant nonlinear plant and a fixed control law. Time-varying plants, gain-scheduled controllers, and adaptive control laws are not covered by the current framework. Extending the results to these cases would require time-varying versions of the storage inequality and Lipschitz conditions, which is left for future work.

4- The interference model may not capture all finite-register effects:

The sector-bounded interference operator of Assumption 4 models a broad family of finite-precision distortions but does not explicitly capture overflow wraparound, deadband effects in fixed-point arithmetic, or limit cycles in recursive digital filters. For systems where overflow is a dominant concern — such as high-gain controllers implemented on short word-length processors — the model of Assumption 4 may be insufficient and more specialized overflow nonlinearity models should be used instead.

5- No delay or packet loss:

The framework does not account for computation delays, network-induced delays, or packet dropouts in networked control systems. In practice, digital controllers always have some computation delay between measurement and actuation. Even a one-step delay can significantly affect stability, especially at fast sampling rates. Engineers implementing the results of this paper in a networked or embedded system with non-negligible computation time must account for this separately.

6- Bounds are conservative for strongly nonlinear systems:

The theoretical bounds are derived using global Lipschitz constants and worst-case error estimates. For strongly nonlinear systems where the Lipschitz constant varies significantly with the operating point, the bounds may be overly conservative — as much as 15 percent in the benchmarks shown here, and potentially more for systems with wider operating ranges or sharper nonlinearities. Semi-global or local versions of the results may give tighter bounds for such cases.

7- No stochastic or probabilistic treatment:

Quantization errors and finite-register distortions are treated as deterministic bounded disturbances. In practice, quantization noise is often modeled stochastically, and probabilistic stability guarantees (almost sure convergence, mean-square stability) may be more appropriate for certain applications. The current deterministic framework provides worst-case guarantees, which are safe but potentially conservative compared to stochastic approaches.

6.4 Practical warnings

From the above limitations, it is important to heed the following warnings when using this approach:

1- Always verify the Lipschitz constants over the full operating regions, not just locally near the equilibrium. If not available analytically, use interval arithmetic or sum-of-squares solvers.

2- Do not use the design inequalities of Corollary 1 outside the region where the storage function V meets Assumption 2. Closing the loop near the saturation limits or where the nonlinearities are large may affect the Lipschitz bounds used in the analysis.

3- Explicitly test for overflow on a fixed-point computer. If the state or control exceed the numerical range of the processor, the model of interferences in Assumption 4 is invalid, and the stability results no longer hold. Provide saturation protection at processor level.

4- If the control law is a recursive algorithm (for example, integral action, dynamic output feedback), limit cycles caused by finite word lengths may result that are not anticipated by this model. In that case, use deadband compensation or dithering, in addition to the quantization level design in Corollary 1.

5- The residual bound r_f is a worst-case bound. In most cases, the steady-state error will be less than rf, as is shown in the simulation ratios of 0.855 to 0.967 in Table 1. However, the worst-case bound should still be used for safety-critical design decisions.

6- For networked implementations, the computation delay between measurement acquisition and control signal application must be modeled separately. Even a single sampling period delay introduces an additional error term in the storage inequality that can significantly increase the residual bound beyond the values predicted by the current analysis.

6.5 Future research directions

Several extensions of the proposed framework are open for future investigation:

Extension to networked control systems with communication delays and packet losses, where the implementation perturbation includes delay-induced discrepancies between intended and applied control signals.

Incorporation of event-triggered implementations, where quantization and finite-register effects interact with the triggering condition in ways that may reduce or increase the residual bound.

Application to multi-agent formation control and robotic manipulators, where the plant nonlinearities and implementation constraints are well characterized. Development of adaptive and dynamic quantization schemes that reduce the residual set size by zooming in as the state converges, combined with the passivity analysis of this paper.

REFERENCES

[1] de Souza, C.E., Coutinho, D.F., Fu, M. (2010). Stability analysis of finite-level quantized discrete-time linear control systems. European Journal of Control, 16(3): 258-271. https://doi.org/10.3166/ejc.16.258-271

[2] Guo, M., Dimarogonas, D.V. (2013). Consensus with quantized relative state measurements. Automatica, 49(8): 2531-2537. https://doi.org/10.1016/j.automatica.2013.05.001

[3] Sun, H.Y., Han, H.G., Qiao, J.F. (2023). Quantized sampled-data stabilization for nonlinear NCSs subject to successive packet losses and probabilistic sampling.

IEEE Transactions on Fuzzy Systems, 32(3): 969-978. https://doi.org/10.1109/TFUZZ.2023.3315722

[4] Han, X., Cheng, N., Ma, Y. (2018). Sampled-data control for TS fuzzy systems with quantized signals. In 2018 IEEE 7th Data Driven Control and Learning Systems Conference (DDCLS), Enshi, China, pp. 145-149. https://doi.org/10.1109/DDCLS.2018.8516042

[5] Oncoy, D.J., Cardim, R., Teixeira, M.C., Faria, F.A., Assuncao, E., Lazarini, A.Z. (2023). New stabilization conditions for fuzzy-based sampled-data control systems using a fuzzy Lyapunov functional. IEEE Access, 11: 15390-15403. https://doi.org/10.1109/ACCESS.2023.3245026

[6] Ren, W., Xiong, J. (2019). Tracking control of nonlinear networked and quantized control systems with communication delays. IEEE Transactions on Automatic Control, 65(8): 3685-3692. https://doi.org/10.1109/TAC.2019.2949102

[7] Pulikonda, M., Kokil, P. (2026). Stability of discrete-time system employing quantization and overflow nonlinearities. Transactions of the Institute of Measurement and Control, 48(1): 112-121. https://doi.org/10.1177/01423312241281072

[8] Pulikonda, M., Kokil, P. (2024). Stability of interfered discrete-time system with concatenations of quantization and overflow. Circuits, Systems, and Signal Processing, 43(1): 302-317. https://doi.org/10.1007/s00034-023-02467-3

[9] Pulikonda, M., Kokil, P. (2024). New results on generalized dissipativity analysis of discrete system with overflow nonlinearity. IFAC-PapersOnLine, 57: 60-65. https://doi.org/10.1016/j.ifacol.2024.05.011

[10] Tokaji, I. (1986). Non-minimal state-space realizations of digital filters (roundoff error, spectral decomposition, unit noise gain, l (2)-scaling). University of California, Irvine.

[11] Ozay, N., Gupta, V., Xu, X. (2020). Passivity-based analysis of sampled and quantized control implementations. Automatica, 119: 109064. https://doi.org/10.1016/j.automatica.2020.109064

[12] Persis, C.D., Jayawardhana, B. (2012). Coordination of passive systems under quantized measurements. SIAM Journal on Control and Optimization, 50(6): 3155-3177. https://doi.org/10.1137/110844994

[13] Yao, L., Huang, X., Wang, Z., Xia, J., Shen, H. (2021). Passivity-based stochastic sampled-data control of Markovian jump systems via looped-functional approach. International Journal of Robust and Nonlinear Control, 31(12): 5665-5679. https://doi.org/10.1002/rnc.5563

[14] Ji, Y., Wu, W., Fu, H., Qiao, H. (2021). Passivity-based filtering for networked semi-Markov robotic manipulators with mode-dependent quantization and event-triggered communication. International Journal of Advanced Robotic Systems, 18(2): 1729881420939864. https://doi.org/10.1177/1729881420939864

[15] Chen, G., Sun, J., Chen, J. (2018). Passivity-based robust sampled-data control for Markovian jump systems. IEEE Transactions on Systems, Man, and Cybernetics: Systems, 50(7): 2671-2684. https://doi.org/10.1109/TSMC.2018.2825474

[16] Zhu, F., Yu, H., McCourt, M.J., Antsaklis, P.J. (2012). Passivity and stability of switched systems under quantization. In Proceedings of the 15th ACM International Conference on Hybrid Systems: Computation and Control, Beijing, China, pp. 237-244. https://doi.org/10.1145/2185632.2185668

[17] Di Ferdinando, M., Di Gennaro, S., Bianchi, D., Pepe, P. (2024). On robust quantized sampled-data tracking control of nonlinear systems. IEEE Transactions on Automatic Control, 69(10): 7120-7127. https://doi.org/10.1109/TAC.2024.3393119

[18] Dong, J., Yang, G.H. (2008). H∞ control for fast sampling discrete-time singularly perturbed systems. Automatica, 44(5): 1385-1393. https://doi.org/10.1016/j.automatica.2007.10.010

[19] Zhang, Y., Liang, H., Xia, Y., Yan, J. (2025). Stabilization for fast sampling discrete-time singularly perturbed singular Markovian systems. Automatica, 171: 111981. https://doi.org/10.1016/j.automatica.2024.111981

[20] Wang, Y., Leduc, R.J. (2012). Sampled-data controller implementation. International Journal of Control, 85(9): 1343-1360. https://doi.org/10.1080/00207179.2012.684248

[21] Grüne, L., Müller, M.A., Kellett, C.M., Weller, S.R. (2020). Strict dissipativity for discrete time discounted optimal control problems. Mathematical Control and Related Fields (MCRF), 11: 771-796. https://doi.org/10.15488/16458

[22] Chang, L., Fu, C. (2023). Designing a stabilizing controller for discrete-time nonlinear feedforward systems with unknown input saturation. International Journal of Robust and Nonlinear Control, 33(3): 2078-2089. https://doi.org/10.1002/rnc.6502

[23] Pang, H., Liu, S., Li, C. (2023). Semi-passivity and practical stability for switched discrete-time nonlinear systems. Franklin Open, 3: 100021. https://doi.org/10.1016/j.fraope.2023.100021

[24] Kawano, Y., Moreschini, A., Cucuzzella, M. (2023). Symplectic discrete-time Krasovskii passivity-based control for output consensus. IFAC-Papers OnLine, 56: 8562-8567. https://doi.org/10.1016/j.ifacol.2023.10.017

[25] Blanchini, F. (2002). Ultimate boundedness control for uncertain discrete-time systems via set-induced Lyapunov functions. IEEE Transactions on automatic Control, 39(2): 428-433. https://doi.org/10.1109/9.272351

[26] Liu, T., Jiang, Z.P. (2018). Event-triggered control of nonlinear systems with state quantization. IEEE Transactions on Automatic Control, 64(2): 797-803. https://doi.org/10.1109/TAC.2018.2837129

[27] Moreschini, A., He, W., Ortega, R., Lu, Y., Li, T. (2026). Globally stable discrete time PID passivity-based Control of power converters: Simulation and experimental results. Automatica, 189: 112976. https://doi.org/10.48550/arXiv.2508.18719

[28] Chopra, N., Fujita, M., Ortega, R., Spong, M.W. (2022). Passivity-based control of robots: Theory and examples from the literature. IEEE Control Systems Magazine, 42(2): 63-73. https://doi.org/10.1109/MCS.2021.3139722